JOURNAL OF SYNCHROTRON RADIATION

ISSN 1600-5775

# A deformation rig for synchrotron microtomography studies of geomaterials under conditions down to 10 km depth in the Earth

**François Renard,[a,b]* Benoit Cordonnier,[a] Dag K. Dysthe,[a] Elodie Boller,[c] Paul Tafforeau[c] and Alexander Rack[c]**

[a]Departments of Geosciences and Physics, PGP, University of Oslo, Box 1048, Blindern, Oslo 0316, Norway, [b]ISTerre, Université Grenoble Alpes and CNRS, CS40700, Grenoble 38058, France, and [c]ESRF – The European Synchrotron, CS40220, Grenoble 38043, France. *Correspondence e-mail: francois.renard@geo.uio.no

Received 5 March 2016
Accepted 30 May 2016

Edited by A. Momose, Tohoku University, Japan

**Keywords:** microtomography; *in situ* studies; porous media; hard X-rays.

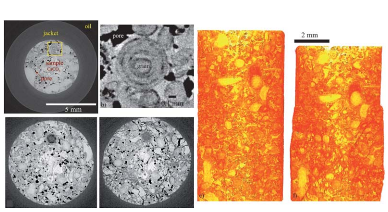



A hard X-ray transparent triaxial deformation apparatus, called HADES, has been developed by Sanchez Technologies and installed on the microtomography beamline ID19 at the European Radiation Synchrotron Facility (ESRF). This rig can be used for time-lapse microtomography studies of the deformation of porous solids (rocks, ceramics, metallic foams) at conditions of confining pressure to 100 MPa, axial stress to 200 MPa, temperature to 250°C, and controlled aqueous fluid flow. It is transparent to high-energy X-rays above 60 keV and can be used for *in situ* studies of coupled processes that involve deformation and chemical reactions. The rig can be installed at synchrotron radiation sources able to deliver a high-flux polychromatic beam in the hard X-ray range to acquire tomographic data sets with a voxel size in the range 0.7–6.5 µm in less than two minutes.

## 1. Introduction

Several groups have studied the three-dimensional deformation of geomaterials and rocks with two main goals: characterizing the static or dynamic evolution of three-dimensional microstructures (Desrues *et al.*, 1996; Bésuelle *et al.*, 2000; Renard *et al.*, 2004, 2009; Fusseis *et al.*, 2009; Zhu *et al.*, 2011; Okumura *et al.*, 2015), and using microtomography data to calculate petrophysical properties, transport properties and deformation fields [Arns *et al.*, 2002; Degruyter *et al.*, 2010; see also reviews by Cnudde & Boone (2013) and Fusseis *et al.* (2014*a*)]. Several years ago, a rig was developed to study the *in situ* deformation of soft rocks at very shallow depth conditions (1 MPa pressure) and room temperature (Viggiani *et al.*, 2004). Another apparatus (Fusseis *et al.*, 2014*b*) has been developed and used at the Advanced Photon Source (Argonne National Laboratory, USA) to deform rock samples. It can reach a pressure of 20 MPa, a temperature of 200°C and reproduce thermodynamic conditions observed in shallow geological reservoirs. In both cases, the thermodynamic conditions correspond to those in shallow crustal environments, *i.e.* less than 2 km depth. However, several geological processes occur in ranges of depths larger than those achieved so far in these experiments: earthquake nucleation (5–20 km depth), diagenesis of sediments (2–10 km depth), maturation of organic matter and primary migration of hydrocarbon geo-resources (3–10 km depth), geological sequestration of carbon dioxide (1–3 km depth) and metamorphic reactions (10–30 km depth). We present here a triaxial deformation rig where 5 mm-diameter core samples of rocks or other porous or non-porous materials can be imaged using hard X-ray microtomography while being deformed under controlled conditions. The HADES rig is designed to load a solid sample at stress and temperature conditions relevant for studies of geomaterials at depths up to 10 km in the Earth's crust.

## 2. The HADES triaxial deformation rig

The equipment is composed of (1) the main body of the triaxial rig (Fig. 1), (2) two pumps that control the axial load and the confining pressure, (3) two pumps that control the pore fluid, (4) a heating system integrated into the rig, (5) two cabinets with the electronics, (6) a computer with the software and a graphical user interface (Fig. 2). The equipment is currently installed on beamline ID19 at the ESRF, with the rig, pumps and controllers located in the hutch and the computer located in the user control room.

The body of the rig (Fig. 1) is machined from a single piece of titanium and the wall thickness in front of the sample is 5 mm, thick enough to resist a confining pressure up to 100 MPa during heating up to 250°C. The triaxial rig and the pumps controlling axial and confining pressures are attached to a base plate which fits the rotating system of the beamline (Fig. 2). To ensure a 180° rotation, outlet connectors for pressure sensor signal, temperature probes, motors power supply and heating elements are connected with two slip rings. The top slip ring connects the top heating system and temperature probes, whereas the bottom slip ring connects the pumps control, the pressure sensors and the bottom heating system. The cumulated torque of these two slip rings is smaller than the limit of 1 N m, required by the motor of the tomograph rotating stage, which is an air-bearing system (Leuven Air Bearings RT250).

All the controlling systems of the rig, including those of the axial and confining syringe pumps, are embedded in two different cabinets. Each cabinet integrates two electronics PID controllers. The first one (MCAPC) is dedicated to the pump control, the second one (MCAT) is dedicated to the control of the heaters. Supervision of the whole system is managed by a control software based on the open source code *Falcon*. The graphical user interface is shown in Fig. 2(*c*).

The rig is a silicon oil liquid confined system. Confining and axial pressures are performed and controlled with two micro pumps, each of 20 ml capacity. They may be used with either constant pressure or constant flow rate modes with predefined ramps. Under room temperature the pressure capacity is certified from 0.1 to 100 MPa with a maximal uncertainty of 0.05 MPa. Concerning the confining pressure, a compensation chamber connected to the sample assembly chamber ensures that the axial and radial stresses applied on the sample are in equilibrium (Fig. 1*b*). Hence, the axial stress can be assumed directly as a differential stress with a maximum value of 200 MPa.

The thermal operating range of the rig spans from room temperature to 250°C with a maximal uncertainty of 1°C.

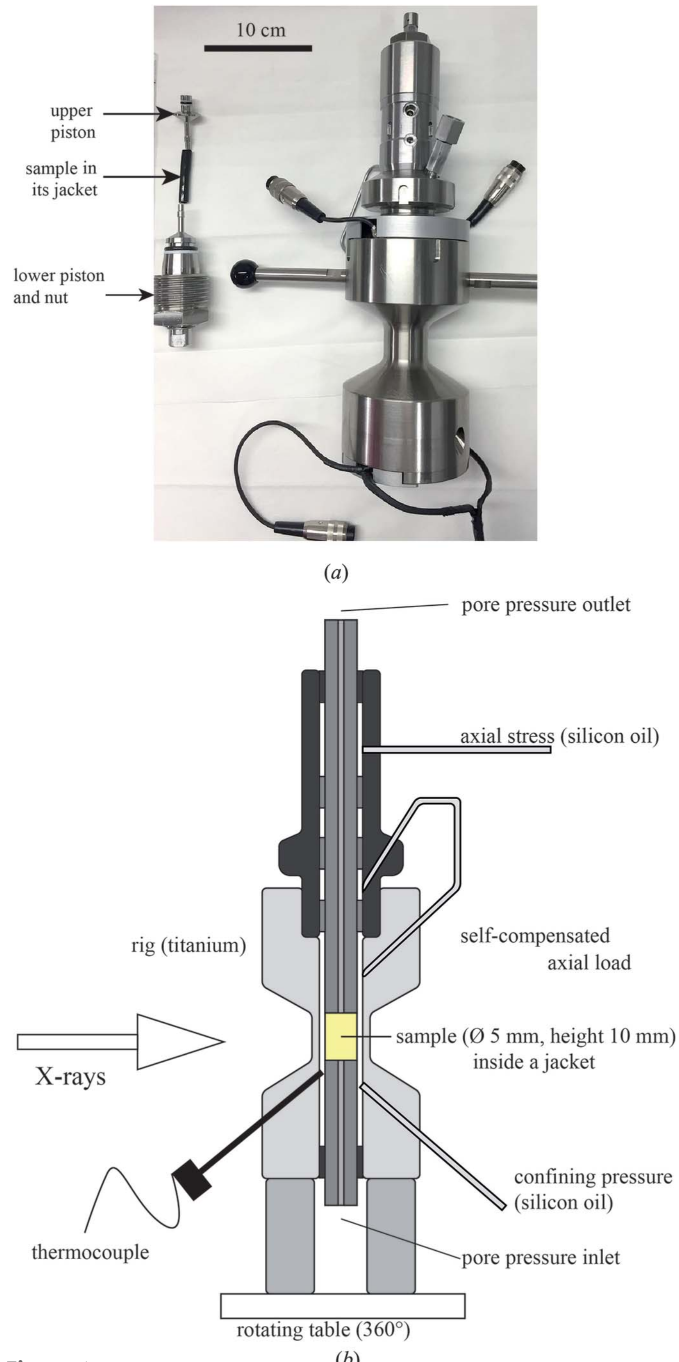


**Figure 1**
Main body of the HADES rig. (*a*) Sample assembly and body of the rig. (*b*) Cross section of the rig.

Heating is controlled by two thermo-resistances inserted in the top and the bottom of the rig. The whole cell body heats up the confining fluid homogeneously ensuring the thermal gradients in the sample are minimized. The thermal regulation is controlled by a type J thermocouple (−40 to +750°C) in direct contact with the jacket and located 8 mm below the sample. The top and the bottom heaters are monitored with two additional thermocouples at the base and the top of the sample assembly chamber.

The pore fluid system is controlled with two Stigma pumps, the first one for the inlet pore fluid and the second one for the

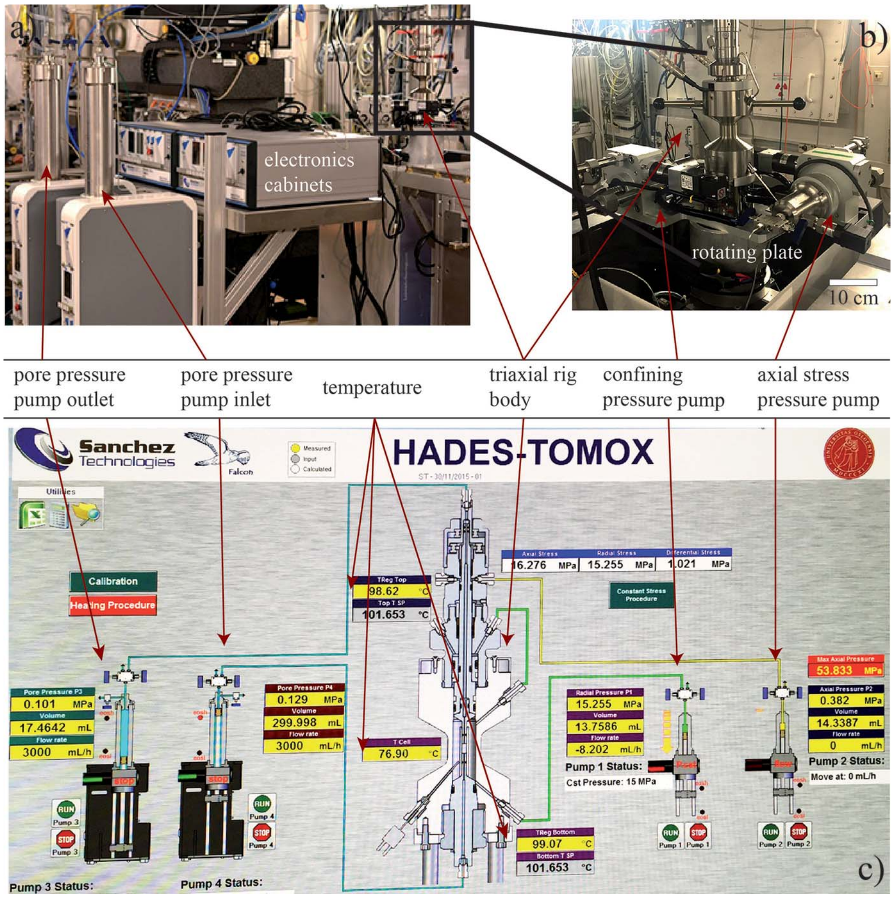


**Figure 2**
HADES triaxial deformation rig installed on beamline ID19 at the ESRF. (*a*) View of the equipment with the rig, the electronics and the pore pressure pumps. (*b*) Main body of the rig shown in Fig. 1. (*c*) Graphical user interface for the controls. Arrows point to the various components of the equipment and their counterparts in the graphical user interface.

outlet. Both pumps have a capacity of 300 ml. They may be used in either constant pressure or constant flow rate modes with predefined ramps. Under room temperature the pressure capacity is certified from 0.1 to 100 MPa with a maximal uncertainty of 0.01 MPa. The flow rate certification is from 10 to 100 ml min$^{-1}$ with a maximal uncertainty of 0.05 ml min$^{-1}$. Each pump has a total dimension of 1 m × 1 m × 0.5 m and a weight of 40 kg. The certified temperature range is from 0 to 40°C but an extended range may be used to the limits of the sealing O-rings. Each pump is equipped with three outlets which allow controlled liquid/gas mixing. Independent control for each pump allows various permeability tests such as continuous flow rate, constant flow rate under controlled pressure or differential pressure.

Inside the rig, the assembly is composed of the sample, embedded into a jacket, and installed between two pistons. Samples are cylinders 10 mm long and with a 5 mm diameter. The whole sample assembly (Fig. 1*a*) is encased into a Viton rubber jacket, 50 mm long and 1.5 mm thick, which ensures a perfect sealing between the confining fluid and the sample assembly. When installed in the rig, the sample is confined by silicon oil and the confining and axial pressure chambers are isolated through a set of O-rings made either in Viton (for experiments at temperatures below 100°C) or Vespel (for experiments up to 250°C).

## 3. Data acquisition

This rig is installed on a medium-resolution CT scanner where the maximum possible weight tolerable by the mechanics is 30 kg, above the 25 kg weight of the rig and its pumps. In addition, two translation stages are used to center the sample with respect to the vertical rotation axis. Because the experiments require relatively fast scans, high-energy polychromatic beam configurations are mandatory, with a large field of view. Among the different insertion devices available on ID19 (undulators U13, U17.6, two U32, and wiggler W150m), the wiggler is the most suitable when imaging with the full field of view of the detector is required (typically scans in the 6.5 µm range). This insertion device delivers a large, intense and (partially) coherent beam using a wiggler gap of 60 mm, with a photon flux density above $10^{10}$ photons mm$^{-2}$ s$^{-1}$ (Sanchez *et al.*, 2013). The beam is rectangular (5 mm × 10 mm, defined by slits upstream of the experimental hutch) to image the whole sample inside the rig. The rig itself and two 2.8 mm-thick aluminium plates are used to filter the lower range of the spectrum of the full synchrotron beam. As a result, an average energy of 93 keV, with peak energy 80 keV and bandwidth (FWHM) 61–110 keV, is transmitted through the rig and sample assembly. U32 undulators coupled with refractive lenses can be used also on ID19 when higher resolution is required. These insertion devices can produce polychromatic beam with high enough energy, but on a smaller field of view (maximum 5 mm in vertical direction). The main interest compared with the wiggler in this case is a better control of the X-ray spectrum with a narrower spectrum, and less high-energy scattering in general.

A 1× magnification optics (two Hasselblad lenses in tandem-like configuration) equipped with a 1 mm-thick GGG:Eu (Eu-doped $Gd_3Ga_5O_{12}$) scintillator and coupled to a commercial sCMOS camera (pco.edge 5.5 with 2560 × 2160 pixels, 6.5 µm pixel size, PCO AG, Germany) is used at a sample–detector distance of 1.3 m to benefit from both absorption and phase contrasts (Cloetens *et al.*, 1996). Other detectors can be used to reach voxel sizes down to 0.7 µm and are still able to operate with a high-energy high-flux polychromatic beam. Tomography acquisitions are driven by commercial and ESRF-developed control softwares, *i.e.* a combination of *SPEC* with in-house-developed device servers for the camera control. For the tomographic acquisition, continuous rotation of the sample is preferred: the corresponding synchronization with the camera is based on the angular encoder signal of the rotation stage. A common exposure time is 0.02 s and 2500 projections are taken over 180°, resulting in a total scan time of about 65 s (200 mA-based operation of the ESRF storage ring), which ensures that the processes are followed in the sample at a frequency of 0.015 Hz. By tuning the detector configuration and properties, it is possible either to increase quality data at slow speed with high-dynamic setup, or to reduce the duration of the scans down to a few seconds by working with lower dynamic systems. For tomographic reconstruction using plain filtered back-projection, the program *PyHST2* is used (Mirone *et al.*, 2014), coupled with a single-distance phase-retrieval process adapted from Paganin *et al.* (2002) (see also Sanchez *et al.*, 2012).

So far, the rig has been calibrated during a series of off-line tests to control temperature, pressure stability and pore pressure. The rig has been successfully used in several on-line deformation experiments, all of which are still being analyzed: (1) deformation of a porous limestone (Anstrude quarry, France) at 20 MPa confining pressure and up to 100 MPa axial stress until ductile deformation (Fig. 3); (2) deformation of a porous limestone (Anstrude) at 5 MPa confining pressure and up to 50 MPa axial stress until formation of a shear brittle fracture; (3) deformation of a sandstone (Adamswiller) at 30 MPa confining pressure and up to 135 MPa axial stress until formation of a shear fracture; (4) deformation of a Green River shale at 20 MPa confining pressure and up to 150 MPa axial stress until formation of two shear fractures.

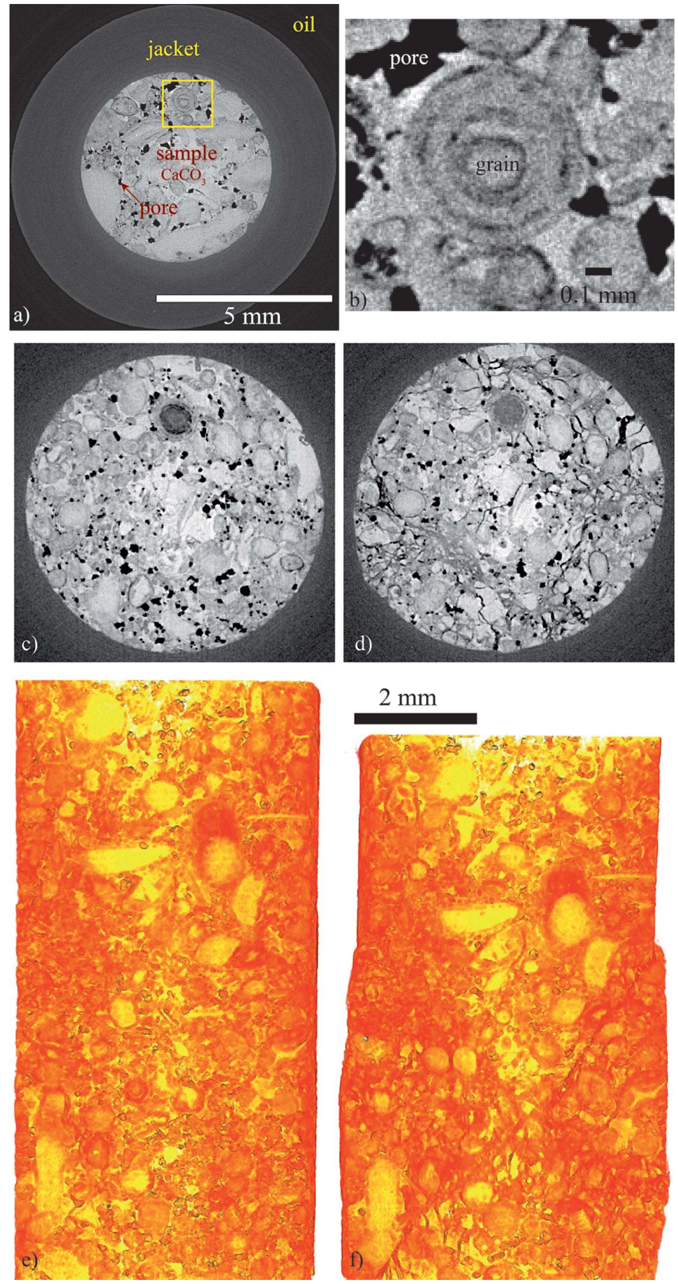


**Figure 3**
(*a*) Reconstructed slice of a limestone sample (Anstrude quarry, France) inside the rig at a voxel resolution of 6.5 µm. The sample is under a 20 MPa confinement and a 22 MPa axial load. The calcite grains appear in light grey, whereas the pores are dark. The jacket and the confining oil are indicated. (*b*) Zoom inside the sample corresponding to the yellow box in (*a*). (*c*), (*d*) Slice in the sample before (*c*) and after (*d*) deformation at 85 MPa, where the sample has ruptured and microfractures are visible, as well as pore collapse. (*e*), (*f*) Rendering of the sample before (*e*) and after (*f*) rupture, where the main shear fault is visible.

## 4. Conclusion

A deformation rig is presented here that allows conditions of stress, temperature and fluid flow to be reproduced similar to those in rocks of the Earth's upper crust, while performing time-lapse microtomography imaging. This rig, installed on beamline ID19 at the ESRF, requires a high-flux polychromatic beam with a photon energy above 60 keV. Voxel sizes in the range 0.7–6.5 µm can be applied. The scan duration can be as short as one minute under such conditions, but scans in the few seconds range could also be performed for some configurations. The HADES rig contributes to a better understanding of geological processes and could also be used in materials science. The device is accessible within the standard users' programme of beamline ID19 at ESRF.

## Acknowledgements

Use of the European Radiation Synchrotron Facility was supported through a Long-Term Proposal (ES-295). The HADES rig was funded by an infrastructure grant from the University of Oslo. We thank Jeroen Jacobs and Bernard Gorges (ESRF) for valuable advice during the conception of the rig. Sébastien Sanchez, Aurélie Pondelek and Cédric Froment from Sanchez Technologies designed and constructed the deformation rig.

## References

Arns, C. H., Knackstedt, M. A., Pinczewski, W. V. & Garboczi, E. J. (2002). *Geophysics*, **67**, 1396–1405.

Bésuelle, P., Desrues, J. & Raynaud, S. (2000). *Int. J. Rock Mech. Min. Sci.* **37**, 1223–1237.
Cloetens, P., Barrett, R., Baruchel, J., Guigay, J.-P. & Schlenker, M. (1996). *J. Phys. D*, **29**, 133–146.
Cnudde, V. & Boone, M. N. (2013). *Earth Sci. Rev.* **123**, 1–17.
Degruyter, W., Burgisser, A., Bachmann, O. & Malaspinas, O. (2010). *Geosphere*, **6**, 470–481.
Desrues, J., Chambon, R., Mokni, M. & Mazerolle, F. (1996). *Géotechnique*, **46**, 529–546.
Fusseis, F., Regenauer-Lieb, K., Liu, J., Hough, R. M. & De Carlo, F. (2009). *Nature (London)*, **459**, 974–977.
Fusseis, F., Steeb, H., Xiao, X., Zhu, W., Butler, I. B., Elphick, S. & Mäder, U. (2014*b*). *J. Synchrotron Rad.* **21**, 251–253.
Fusseis, F., Xiao, X., Schrank, C. & De Carlo, F. (2014*a*). *J. Struct. Geol.* **65**, 1–16.
Mirone, A., Brun, E., Gouillart, E., Tafforeau, P. & Kieffer, J. (2014). *Nucl. Instrum. Methods Phys. Res. B*, **324**, 41–48.
Okumura, S., Uesugi, K., Nakamura, M. & Sasaki, O. (2015). *J. Geophys. Res. Solid Earth*, **120**, 2974–2987.
Paganin, D., Mayo, S. C., Gureyev, T. E., Miller, P. R. & Wilkins, S. W. (2002). *J. Microsc.* **206**, 33–40.
Renard, F., Bernard, D., Desrues, J. & Ougier-Simonin, A. (2009). *Earth Planet. Sci. Lett.* **286**, 285–291.
Renard, F., Bernard, D., Thibault, X. & Boller, E. (2004). *Geophys. Res. Lett.* **31**, L07607.
Sanchez, S., Ahlberg, P. E., Trinajstic, K., Mirone, A. & Tafforeau, P. (2012). *Microsc. Microanal.* **18**, 1095–1105.
Sanchez, S., Fernandez, F., Pierce, S. E. & Tafforeau, P. (2013). *Nat. Protoc.* **8**, 1708–1717.
Viggiani, G., Lenoir, N., Bésuelle, P., Di Michiel, M., Marello, S., Desrues, J. & Kretzschmer, M. (2004). *C. R. Méc.* **332**, 819–826.
Zhu, W., Gaetani, G. A., Fusseis, F., Montési, L. G. & De Carlo, F. (2011). *Science*, **332**, 88–91.